Stabilizing Perovskite Precursor by Synergy of Functional Groups for NiOx-Based Inverted Solar Cells with 23.5 % Efficiency

Mengjia Li, Haiyun Li, Qixin Zhuang, Dongmei He, Baibai Liu, Cong Chen, Boxue Zhang, Thierry Pauporté, Zhigang Zang, Jiangzhao Chen

Cite this paper as: M. Li, H. Li, Q. Zhuang, D. He, B. Liu, C. Chen, B. Zhang, T. Pauporté, Z. Zang, and J. Chen,
Stabilizing Perovskite Precursor by Synergy of Functional Groups for NiO_x-Based Inverted Solar Cells with 23.5% Efficiency.
Angew. Chem. Int. Ed., 61 (2022) e202206914. DOI: 10.1002/anie.202206914

Stabilizing Perovskite Precursor by Synergy of Functional Groups for NiOx-Based Inverted Solar Cells with 23.5% Efficiency

Mengjia Li[1#], Haiyun Li[2#], Qixin Zhuang[2]#, Dongmei He[2], Baibai Liu[2], Cong Chen[1,4*], Boxue Zhang[3], Thierry Pauporté[3], Zhigang Zang[2*], and Jiangzhao Chen[2*]

1 State Key Laboratory of Reliability and Intelligence of Electrical Equipment, School of Material Science and Engineering, Hebei University of Technology, Dingzigu Road 1, Tianjin 300130, People' s Republic of China.

2 Key Laboratory of Optoelectronic Technology & Systems (Ministry of Education), College of Optoelectronic Engineering, Chongqing University, Chongqing 400044, China

3 Chimie ParisTech, PSL Research University, CNRS, Institut de Recherche de Chimie Paris (IRCP), UMR8247, 11 rue P. et M. Curie, F-75005 Paris, France

4 Macao Institute of Materials Science and Engineering (MIMSE), Macau University of Science and Technology, Taipa, Macau SAR, 999078 China

#These authors contributed equally to this work.

∗ Corresponding authors. E-mail: chencong@hebut.edu.cn, zangzg@cqu.edu.cn, jiangzhaochen@cqu.edu.cn

Abstract

Perovskite solar cells suffer from poor reproducibility due to the degradation of perovskite precursor solution. Herein, we report an effective precursor stabilization strategy via incorporating 3-hydrazinobenzoic acid (3-HBA) containing carboxyl (-COOH) and hydrazine (-$NHNH_2$) functional groups stabilizer. The oxidation of I^-, deprotonation of organic cations and amine-cation reaction are main causes of the degradation of mixed organic cation perovskite precursor solution. The -NHNH2 can reduce I_2 defects back to I^- and thus suppress the oxidation of I^-, while the H^+ generated by -COOH can inhibit the deprotonation of organic cations and subsequent amine-cation reaction. The above degradation reactions are simultaneously inhibited by the synergy of functional groups.

The inverted device achieves an efficiency of 23.5% (certified efficiency of 23.3%) with excellent operational stability, retaining 94% of the initial efficiency after maximum power point tracking for 601 hours.

Keywords: Perovskite precursor solution; Degradation; Defect passivation; Functional groups; Perovskite solar cells

Introduction

In recent years, organic-inorganic hybrid metal halide perovskite materials have aroused the wide attention of the community and industry due to the advantages of low cost, adjustable band gap, solution processing, high molar extinction coefficient, low exciton binding energy, and high carrier mobility. To date, high-efficiency solution-processed metal halide perovskite solar cells (PSCs) have been reported with a fascinating certified power conversion efficiency (PCE) as high as 25.7%.[1] Although high certified PCE has been obtained, poor reproducibility still poses a serious challenge for the commercial application of perovskite photovoltaic deployment. The whole community has been perplexed by the difficulty for different research groups to reproduce device performance or, for the same person, to get reproducible data from one batch to another. It has been widely reported that the instability of the state of perovskite precursor solution should be primarily responsible for poor reproducibility.[2,3] The aging time dramatically affects the state of perovskite precursor solution (e.g., colloidal size distribution, intermediate phase, type and content of chemical components), which, in turn, affects the morphology, grain size, crystallinity, phase purity, trap state density, and accordingly affects final device performance and reproducibility.[4-7] The state of perovskite precursor solution is mainly affected by colloidal particle structure change caused by solute-solvent coordination, oxidation of iodide ions, deprotonation of organic cations and organic amine-organic cation reaction.[8] A previous report shows that the colloidal particle structure change caused by solute-solvent coordination is reversible, and that it can be controlled by tuning the pH.[9] However, how to effectively suppress the oxidation of iodide ions, deprotonation of organic cations and organic amine-organic cation reaction remains a huge challenge. As the aging time increases, the degradation of the chemical compositions in precursor solution would lead to a deviation from the ideal stoichiometric ratio, which results in a significant device performance difference.[10,11] To address the above issues, there is an urgent need to develop additives to stabilize precursor solution maintaining an accurate stoichiometric ratio between chemical

components, which is crucially important for the fabrication of reproducible, efficient and stable PSCs.

As we mentioned above, the oxidation of iodide ions would lead to instability of perovskite precursor solution. It is well known that iodides (I^-) in metal halide perovskite precursors are readily oxidized into iodine (I_2) during aging. On the one hand, the consumption of I^- ions would make the chemical component ratio in the precursor solution deviate from the ideal stoichiometric ratio. On the other hand, the generated I_2 can serve as carrier nonradiative recombination centers in the subsequently prepared perovskite films and remarkably deteriorates the photovoltaic performance of perovskite devices. To overcome the challenge of the oxidation of iodides, some effective strategies have been proposed. For example, Zhang et al. found that adding hypophosphorous acid into perovskite precursor solution can improve film quality via reducing the I_2 back into I^-.[12] Wang et al. developed a Eu^{3+}–Eu^{2+} redox shuttle to oxidize Pb^0 and reduce I_2, respectively.[13] Chen et al. reported that adding benzylhydrazine hydrochloride into degraded precursor solution can effectively reduce the detrimental I_2 back to I^-.[14] It is worth noting that our group previously developed a multifunctional additive molecule, 4F-PHCl, with reductive hydrazine functional group which can effectively reduce the I_2 defects back into I^- and thus improve photovoltaic performance.[15] The above results indicate that reductant molecules and ions are very effective in healing iodine defects through reducing them back to iodide. Nevertheless, the function of the reported additive molecules is relatively simple, which can only inhibit the oxidation of iodide ions but cannot inhibit the deprotonation of organic cations and the addition and elimination reaction between organic amine and organic cation. In view of this, the development of additive molecules that can simultaneously inhibit the above three reactions is particularly important for completely suppress the degradation of precursor solution, which is key to achieve long-term stability of perovskite precursor solution.

In addition to the oxidation of I^- ions, the degradation of perovskite precursor solution containing formamidinium (FA^+) and methylammonium (MA^+) can also be

triggered by the deprotonation of organic ammonium cation and following addition-elimination reaction.[11] $FAPbI_3$ possesses the narrowest bandgap of 1.45-1.52 eV among all known lead-based metal halide perovskites and has the greatest potential in achieving practical efficiency approaching Shockley-Queisser limit efficiency.[16] Due to the slightly overlarge tolerance factor resulting from the overlarge ionic radius of the FA^+ cation, however, black phase (α-phase) $FAPbI_3$ can easily transform into yellow phase (δ-phase).[17] To stabilize α-phase, a small amount of MA^+ cations with smaller ionic radius than FA^+ are usually employed to partially substitute FA^+ cations in $FAPbI_3$. Presently, most of the state-of-the-art PSCs with efficiencies exceeding 24% are fabricated via using mixed-organic-cation MA^+/FA^+-based perovskites as absorbers.[18] Nevertheless, MA^+/FA^+-based perovskite precursor solution has been revealed to be unstable due to not only the oxidation of I^- ions but also the deprotonation reaction of organic ammonium cation and following addition-elimination reaction.[19] Pang et al reported that volatile methylamine (MA) produced by the deprotonation of MA^+ can react with FAI to form *N*-methyl FAI (MFAI).[3] Subsequently, generated MFAI further reacts with MA to form *N*, *N´*-dimethyl FAI (DMFAI). Colella et al. further confirmed the above degradation route by the amine-cation reaction of MA-FA^+ via powerful nuclear magnetic resonance (NMR) spectroscopy.[11] Recently, Shi et al. also revealed the key role of organoamines from deprotonation reaction of organic ammonium cations (MA^+ and FA^+) in the degradation of mixed MA^+/FA^+ perovskite precursor solution.[8] Slightly different from the conclusions obtained by Pang et al.[3] and Colella et al.[11], however, they demonstrated that the main decomposition route of organic cations is amine-cation reaction of FA-MA^+ instead of amine-cation reaction of MA-FA^+. In any case, amine-cation reaction of MA-FA^+ and/or FA-MA^+ followed by the deprotonation reaction of organic ammonium cations has been certified to be easy to occur. The consumption of small-size MA^+ and the formation of large-size organic cations (MFA^+, $DMFA^+$ and/or FMA^+) over solution aging time would increase the tolerance factor, which results in the formation of yellow δ-phase and

thereby deteriorates film quality and device performance, finally contributing to poor reproducibility.

Since the above degradation reactions markedly affect device performance and reproducibility, some efforts have been devoted to stabilizing precursor solution by suppressing the deprotonation and amine-cation reactions. For instance, Qin et al. introduced ITIC-Th into mixed cations-based perovskite precursor solution to effectively suppress the formation of yellow δ-phase by stabilizing the $[PbI_6]^{4-}$ framework via the coordination bond of Pb with S.[20] Seok et al. incorporated elemental sulfur (S_8) into mixed-cation precursor and demonstrated that S_8 can stabilize precursor solution through inhibiting the deprotonation of MA^+ via amine-sulfur coordination.[21] Pang et al. employed triethyl borate as a stabilizer of mixed-organic-cation perovskite precursor solution and uncovered that the triethyl borate can effectively eliminate the impurity phase by restricting the deprotonation of MAI.[22] Shi et al. effectively suppressed the irreversible degradation route of amine-cation reaction by adding aldehydes into mixed-organic-cation perovskite precursor solution to remove organoamines based on Schiff-base reactions.[23] From the perspective of reaction sequence, organic amine-organic cation reactions can be effectively inhibited as long as deprotonation of organic cations is suppressed. Therefore, it is critical to suppress the deprotonation decomposition reaction of organic cations to thoroughly stabilize perovskite precursor solution. The oxidation of iodide ion, deprotonation of organic cation and reaction of organic amine-organic cation often occur simultaneously in the mixed organic cation precursor. However, the function of presently reported precursor stabilizers is relatively simple, which can only suppress the oxidation of iodide ions, deprotonation of organic cations or irreversible amine-cation reaction. Consequently, it is highly desirable to develop novel additive molecules that can simultaneously inhibit the above three degradation reactions to obtain long-term stable precursor solutions and achieve reliable and reproducible device performance.

PSCs are fabricated as either n-i-p (regular) or p-i-n (inverted) structures.

Recently, inverted PSCs have demonstrated promising PCEs over 24%,[24,25] which is comparable to that of regular devices. In these works, organic hole transport materials (HTM) were adopted, which still would reduce the thermal and light stability of the corresponding solar cells. In contrast, the inverted PSCs based on nickel oxide (NiO_x) inorganic HTM exhibits enormous advantage regarding thermal and operational stability over organic HTMs. To date, a PCE up to 23.1% has been reported for NiO_x-based inverted PSCs.[26] However, the PCE of NiO_x-based inverted PSCs is much lower than that of regular PSCs. The trap-mediated nonradiative recombination resulting from grain boundary (GB) defects is one critical factor impeding the further improvement of the photovoltaic performance of NiO_x-based inverted PSCs.[27,28] In view of this, it is highly expected to develop multifunctional molecules to both stabilize precursor solution and passivate the defects at GBs for the simultaneous enhancement of efficiency, stability, and reproducibility toward commercial application.

In this work, we develop a precursor stabilization and defect passivation strategy by employing 3-hydrazinobenzoic acid (3-HBA) containing both carboxyl (-COOH) and hydrazine (-$NHNH_2$) functional groups as a versatile additive. It is revealed by NMR, X-ray diffraction (XRD), and ultraviolet-visible (UV-vis) absorption techniques that the degradation mechanisms of mixed-organic-cation metal halide perovskite precursor solution mainly involve the oxidation of I^-, the deprotonation of organic cations, and the irreversible degradation route of amine-cation reaction. The oxidation of I^-, deprotonation of organic cations and irreversible amine-cation reaction are demonstrated to be primarily responsible for the degradation of methylammonium- and formamidinium-mixed organic cation perovskite precursor solution. It is demonstrated that the -$NHNH_2$ in 3-HBA can reduce I_2 defects back to I^- and thus suppress the oxidation of I^-. At the same time, it is disclosed that -COOH in 3-HBA as weak acid can produce hydrogen proton by reversible equilibrium ionization reaction. The formed H^+ can inhibit the deprotonation of organic cations and subsequent amine-cation reaction. The

synergistic effect of -$NHNH_2$ and -COOH results in the simultaneous suppression of the above three degradation reactions. Additionally, the 3-HBA can also play a role in passivating grain boundary defects, reducing trap density, and increasing carrier lifetimes regardless of perovskite composition and device configuration. As a result, the resulting NiO_x-based inverted PSC delivers an appealing efficiency of 23.5%, which is the highest value ever reported for a NiO_x-based inverted PSC. The modified devices with 3-HBA maintain 72% of their initial efficiency after aging at 85 ℃ for 672 hours and 94% of their initial efficiency after tracking at maximum power point under continuous illumination for 601 hours. This work provides a simple and effective strategy for precursor solution stabilization and defects passivation through the synergistic effect of organic functional groups and it paves the way for the industrialization of perovskite photovoltaic technology.

Results and discussion

Precursor stability and reproducibility enhancement via 3-HBA

3-HBA containing both -COOH and -$NHNH_2$ functional groups (**Figure 1a**) was directly introduced into fresh triple-cation perovskite ($Cs_{0.05}(FA_{0.83}MA_{0.17})_{0.95}Pb(I_{0.83}Br_{0.17})_3$) precursor solution simultaneously containing FA^+ and MA^+ organic cations, as shown in **Figure 1b**. For clarification purposes, the perovskite precursor solution without 3-HBA is denoted as control solution while the perovskite precursor solution with 3-HBA is denoted as target solution. The photographs of perovskite films fabricated from perovskite precursor solutions without and with 3-HBA at different aging times are exhibited in **Figure 1c**. Obviously, the perovskite films from control and target solutions were very black. The perovskite films from control solutions gradually turned yellow with aging time, and the perovskite film was almost completely yellow upon aging for 75 days. This indicates that precursor solution aging would lead to the formation of yellow δ-phase $FAPbI_3$ due to the consumption of small-size MA^+ and the formation of large-size MFA^+ and $DMFA^+$, which will be discussed thereinafter. In contrast, the

perovskite films from target solutions always maintained a black color even for a PPS aging time of 75 days. It suggests that 3-HBA additive can effectively stabilize PPS and suppress the formation of δ-phase $FAPbI_3$. **Figure 1d and e** present the UV-vis absorption spectra of the perovskite films from control and target solutions aged for different times. The absorption intensity of perovskite films from target solutions was maintained regardless of aging time whereas a significant decrease in absorption intensity over aging time was observed for the perovskite films from control solutions, which is well consistent with the color evolution trend of the perovskite films in **Figure 1c**. X-ray photoelectron spectroscopy (XPS) measurement of the perovskite films from control and target solutions after aging for 75 days was carried out. As displayed in **Figure 1f and g**, the peaks of metallic lead (Pb^0) at 141.35 and 136.49 eV[29] were obviously observed in the perovskite film from the aged

control solution while they were absent in the perovskite film from the aged target solution. This implies that 3-HBA can inhibit the generation of Pb^0 via the coordination between -COOH and undercoordinated Pb^{2+}. In addition, it shows that the hydrazine functional group would not reduce the Pb^{2+} to Pb^0. It can be seen clearly from C 1s spectra in **Figure S1** that the peak of O-C=O at 288.60 eV appears in the perovskite film from aged target solution, which is indicative of the existence of 3-HBA in the final perovskite film.

Steady-state photoluminescence (SSPL) spectra were collected to evaluate the carrier recombination of the perovskite films from the control and target solutions before and after aging for 75 days, as shown in **Figure 1h and i**. We can see that the perovskite film from the aged control solution exhibits remarkably reduced PL intensity than that from the fresh control solution while a similar PL intensity is found for the perovskite films from fresh and aged target solutions. The photograph, UV-vis absorption, and PL results indicate that 3-HBA can effectively stabilize perovskite precursor solution. Interestingly, the PL peak of the perovskite film from the control solution is red-shifted after aging but the same peak position is found for the perovskite films from target solutions before and after aging, which could be

owing to the consumption of MA^+ cations in precursor by deprotonation. This deprotonation process will be confirmed hereafter. To investigate the effect of aging time on device performance, we fabricated NiO_x-based inverted PSCs based on the precursor solutions, with or without 3-HBA stabilizer, and aged for different time (**Figure 1j, k** and **Figure S2**). All photovoltaic parameters of the devices from control solutions reduced significantly as the aging time prolonged. In stark contrast, a slight reduction of all the photovoltaic parameters was observed for the devices from the aged target solutions, even after 75 days, compared to that of the device from the fresh target solution. The above results indisputably suggest that 3-HBA additive efficaciously improves the reproducibility of PSCs by acting as a stabilizer of the precursor solution.

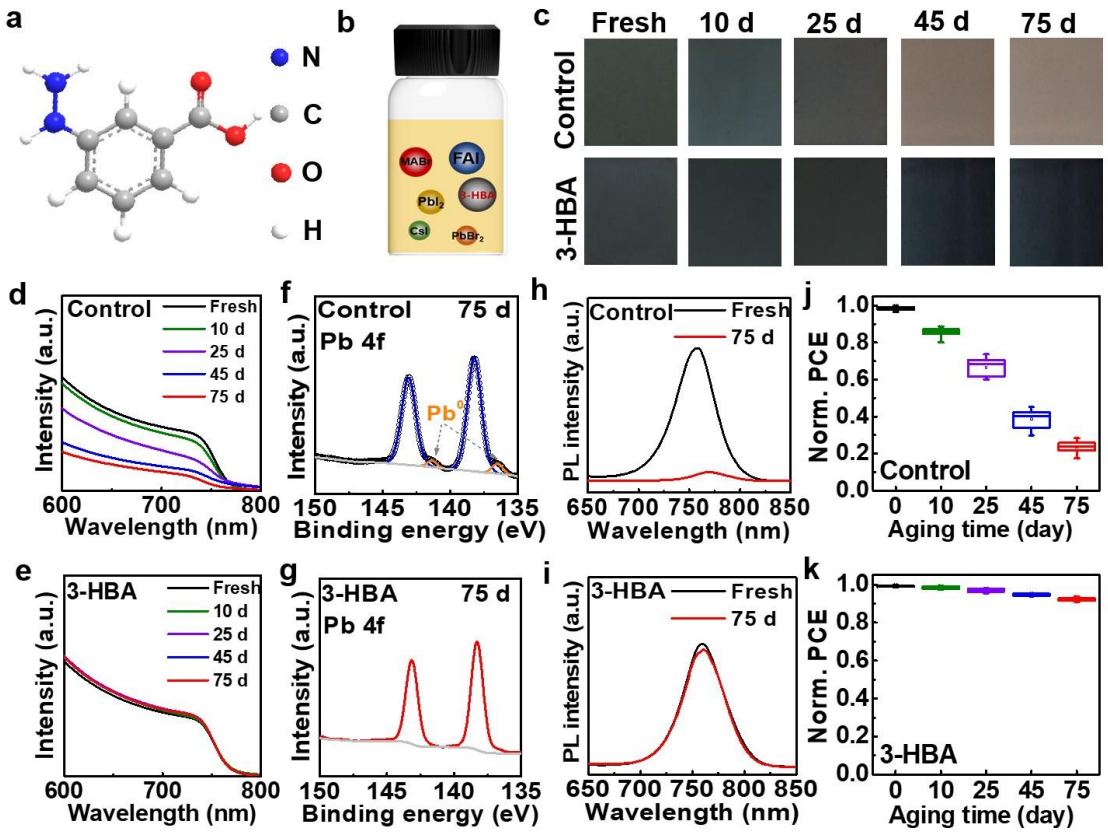

Figure 1. Enhancing precursor stability and device reproducibility. (a) Chemical structure of 3-HBA. (b) Schematic illustration of perovskite precursor solution incorporating 3-HBA. (c) Photographs of the perovskite films prepared by precursor

solutions without and with 3-HBA aged for different times. UV-vis absorption spectra of the perovskite films made by precursor solutions (d) without and (e) with 3-HBA aged for different times. Pb 4f XPS spectra of the perovskite films fabricated from the precursor solutions (f) without and (g) with 3-HBA aged for 75 days. PL spectra of the perovskite films from the solutions (h) without and (i) with 3-HBA before and after being aged for 75 days. PCE evolution of the devices fabricated from precursor solutions (j) without and (k) with 3-HBA aged for different times.

Phase stability improvement of perovskite films by carboxy group

Scanning electron microscopy (SEM) measurement was performed to study the effect of precursor solution aging time on the morphology of perovskite films. **Figure S3** shows a similar morphology for the perovskite films fabricated from fresh control and fresh target solutions. However, the morphology difference gradually enlarged as the aging time increased. Up to the aging time of 25 days, huge morphology differences were perceived for control and target films. Until 75 days, the morphology difference was further markedly magnified. We can clearly see that only small pinholes can be found in the target film while they were huge in the control film. The terrible morphology could be associated with the formation of the impurity phase. The results show that the precursor solution with 3-HBA possesses excellent reproducibility compared with the control solution, which again confirms the stabilization function of 3-HBA for the precursor solution. Subsequently, XRD patterns were measured to evaluate the effect of aging time on the crystal structure and phases of the perovskite films from the control and target precursor solutions, and are reported in **Figure 2a and b**. For the films fabricated from the control precursor solution, a main diffraction peak corresponding to the α-phase located at $\approx$14.2° is gradually weakened with the increase of the aging time. Meanwhile, the diffraction peak at around 11° due to the formation of δ-phase[30] appears in the perovskite films from aged solutions and its intensity gradually increases with the aging time. The enlarged XRD patterns in **Figure 2a** shows a gradual shift tendency toward low diffraction angle with the increase of aging time for the peaks of impurity phase as compared to

the peak position of pure δ-$FAPbI_3$ (11.74°). Itcould be the result of large-size organic cation (MFA^+ and $DMFA^+$) byproducts incorporation into the crystal structure of δ-$FAPbI_3$.[3] In contrast, the introduction of the 3-HBA stabilizer leads to similar intensities of the (110) diffraction peaks due to α-phase for all perovskite films with different aging times (**Figure 2b**). It can be seen from magnified XRD patterns in **Figure 2b** that no impurity δ-phase peak is detected for all perovskite films from target solutions aged for different times. These results suggest that 3-HBA can stabilize mixed-organic-cation perovskite precursor solution by suppressing the formation of δ impurity phase. To clarify the contribution of functional groups in 3-HBA molecules in stabilizing precursor solution, systematic contrast experiments were carried out through adding various additive molecules containing -COOH or -$NHNH_2$ functional groups into precursor solution, including phenylhydrazine (PH), benzoic acid (BA), benzene (C_6H_6), formic acid (HCOOH), m-methylbenzoic acid (3-MBA) and 3-Aminobenzoic acid (3-ABA). As exhibited in **Figure 2c, d**, α-phase can still be observed until 75 days of aging for the perovskite films from solutions with PH or BA. This indicates that both PH and BA can suppress the formation of the δ impurity phase in comparison with the control solution. Nevertheless, PH and BA are much less effective than 3-HBA. A more substantial shift toward a low angle is found for the diffraction peak of the δ impurity phase in the perovskite films from aged solution with PH as compared to that of the δ impurity phase in the perovskite films from aged solution with BA. It means that a larger number of large-size organic cation byproducts is generated in the former film than in the latter film. This proves that -COOH functional group is more effective in suppressing the degradation of organic cations and thus stabilizing precursor solution compared with -$NHNH_2$. It is also found that benzene does not contribute to stabilizing the solution (**Figure 2e**). We also can find that all additive molecules containing -COOH functional groups including HCOOH, 3-ABA, and 3-MBA have almost the same effect as BA in stabilizing solution. Moreover, the -NH_2 and -CH_3 functional groups in the interposition of the benzoic acid barely work (**Figure 2f-h**). This shows that the hydrazine group plays an indispensable role in stabilizing the solution. It can be concluded that -COOH and

-$NHNH_2$ functional groups exhibit synergistic effects in inhibiting the decomposition of organic cations and accordingly the formation of the yellow phase.

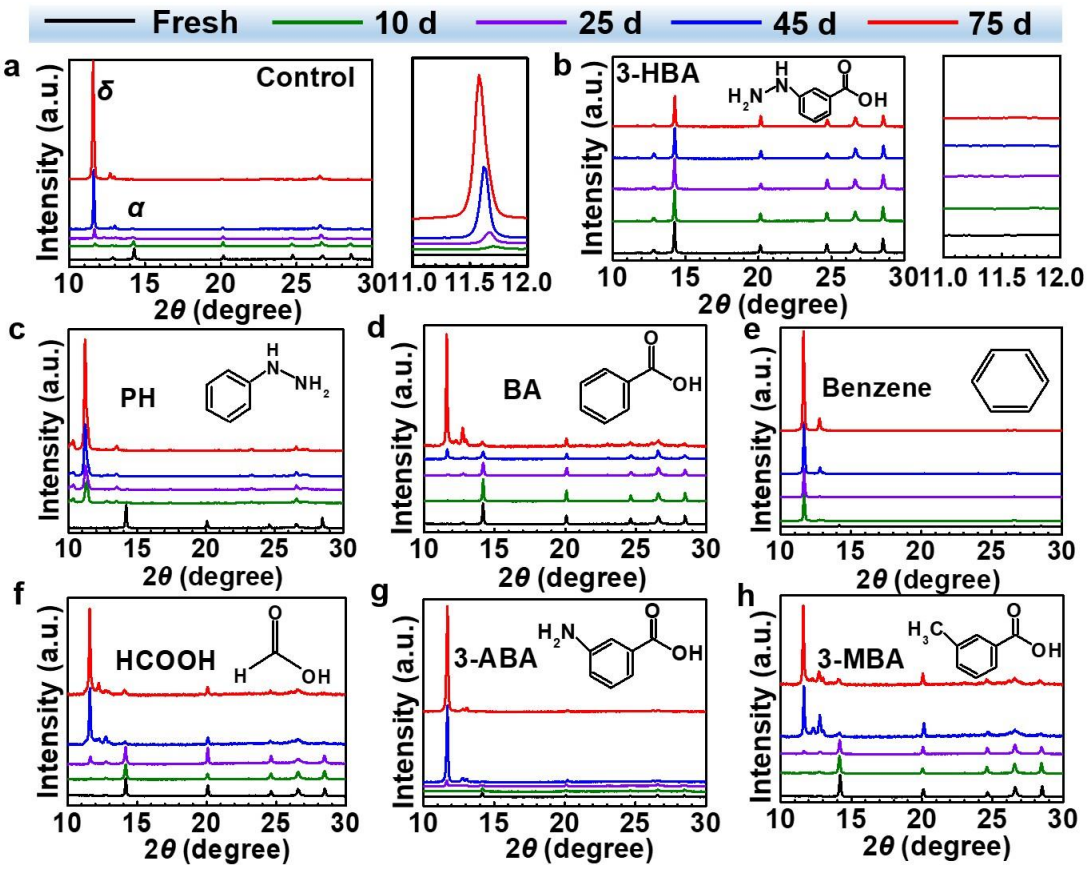

Figure 2. Investigation of the effect of different functional groups on the phase stability of perovskite films. (a) control, (b) with 3-HBA, (c) with PH, (d) with BA, (e) with C_6H_6, (f) with HCOOH, (g) with 3-ABA, and 3-MBA aged for different times. The illustration shows the chemical structures of the additive molecules.

Degradation and stabilization mechanisms of perovskite precursor solution

To further uncover the degradation and inhibiting mechanisms by investigating the evolution of reactants and products, we conducted NMR measurement for the control perovskite precursor solution and modified perovskite precursor solutions with 3-HBA and BA aged in the dark at room temperature for different times (**Figure 3a-c**). The deuterium dimethyl sulfoxide (DMSO-d6) was chosen to avoid the interference of

the residual signals from dimethylformamide (DMF).[11] We observe the peak signals of MA^+ and FA^+ in all solutions regardless of the introduction of additives. The ^1H signal of methyl (CH_3) in MA^+ is at δ = 2.30 ppm and the ^1H signal of methyne (CH) in FA^+ is at δ = 7.78 ppm.[31] The reduction of MA^+ and FA^+ is attributed to the deprotonation of organic cations, which has been certified by previous reports.[32] It is worth noting that some new characteristic peaks appeared and became stronger and stronger in the control solutions as the aging time increases (**Figure 3a**). The ^1H signal peaks at δ = 2.74 and 7.85 ppm belong to MFA^+ and the ^1H signal peak at δ = 2.92 ppm belongs to $DMFA^+$.[31] The formed MA reacts with FA^+ to generate MFA^+ by addition-elimination reaction. Generated MFA^+ can further react with another MA by addition-elimination reaction to form $DMFA^+$. For the sake of discussion, we quantified the reactants (including MA^+ and FA^+) and products (including MFA^+ and $DMFA^+$) by integrating the ^1H signal peaks. The integral results are shown in **Figure S4-S18**. The calculation method for the percentage of each composition is given in **Figure S19**. The percentages of left MA^+, left FA^+, generated MFA^+, and generated $DMFA^+$ in precursor solutions without and with additives are plotted as the aging time in **Figure 3d-g**. Obviously, the amount of MA^+ and FA^+ is maintained at 100% regardless of aging time for the 3-HBA-containing solution while the amount of MA^+ and FA^+ gradually declines with aging time but reduces much more rapidly for the control solution than the BA-containing solution (**Figure 3d, e**). This indicates that 3-HBA completely suppresses the deprotonation of organic cations and the BA is also effective but in a less extend than 3-HBA. It again confirms that -COOH and $-NHNH_2$ play a synergistic role in inhibiting the deprotonation of organic cations, which is in good agreement with the conclusion drawn by XRD results. In addition, the deprotonation of MA^+ is much faster compared to FA^+, which could be due to the weaker alkalinity of the former than the latter. This also proves that MA-based perovskites are usually less stable than the FA-based ones.[33] There is no MFA^+ and $DMFA^+$ in the 3-HBA-containing solution (**Figure 3f, g**), which is reasonable because no MA can be used for the irreversible degradation route of amine-cation reaction since the first step

deprotonation reaction of MA^+ is blocked thoroughly. In contrast, we can observe the generation of MFA^+ and $DMFA^+$ in the aged control solution with an amount which increases with the aging time. However, only MFA^+ can be detected in the aged BA-containing solution with a generation rate which is much slower for the BA-containing solution compared to the control one. Moreover, no $DMFA^+$ is formed in the aged BA-containing solution. It is easy to understand that MFA^+ is more difficult to be generated than $DMFA^+$. In short, we can conclude that -COOH and $-NHNH_2$ can synergistically stabilize precursor solution by suppressing the deprotonation of organic cations and thereby inhibiting the irreversible degradation route of amine-cation reaction. This is indicative of the synergistic engineering of organic functional groups in modulating perovskite precursor solution chemistry. To understand the effect of generated large-size organic cations on phase stability, we calculated the tolerance factor (τ) by the equation $\tau = \frac{r_A + r_X}{\sqrt{2}(r_B + r_X)}$, where r , r , and r represent the ionic radius of A, B, and

X, respectively. The τ is plotted as the substitution ratio of MFA^+ in $FA_{1-x}(MFA)_xPbI_3$ (**Figure 3h**). The pure $FAPbI_3$ has a τ of 0.987 slightly higher than the ideal value, which easily leads to the formation of yellow δ-phase. The τ is enlarged gradually from 0.987 to 1.041 as the substitution ratio increases (**Table S2**). This suggests that doped $FAPbI_3$ perovskite with MFA^+ is less stable than pure $FAPbI_3$. Consequently, the formation of the yellow phase in precursor solution is not only due to the consumption of MA^+ but also to the generation of large-size cations (MFA^+ and $DMFA^+$). In the present work, 3-HBA can suppress the formation of the yellow phase by inhibiting the decomposition of MA^+ and the generation of MFA^+ and $DMFA^+$.

The oxidation of I^- to I_2 is another main degradation route of metal halide perovskite precursor solution.[34] We also explored whether the organic functional groups in 3-HBA molecules can effectively suppress the degradation process through measuring the UV-vis absorption spectra of the commercial HI solutions without and with 3-HBA, PH, or BA additive aged for 75 days. It is well-known that we can still observe the formation of a large amount of I_2 when we open the bottle of commercial HI solution as presented in **Figure S20a**. This shows that I^- is extremely easy to be oxidized to I_2 even if in the presence of a tiny amount of oxygen. As exhibited in **Figure 3i**, very strong peaks at 365 nm are detected for the control and BA-containing HI solutions, which should be ascribed to the generation of I_2 or I_3^-.[35] This suggests that the BA additive only containing -COOH molecule can not suppress the oxidation of I^- to I_2. In contrast, only a very weak peak is observed in the PH-containing HI solution but this peak cannot be detected in the 3-HBA-containing HI solution. This indicates that if both PH and 3-HBA can inhibit the oxidation reaction by reducing I_2 back to I^-, 3-HBA containing -both $NHNH_2$ and -COOH functional groups is slightly more effective than PH which only contains -$NHNH_2$ functional group. The UV-vis absorption result is consistent with the colour change tendency of HI solutions before and after a 75 days aging (**Figure S20**). Up to now, we can conclude that well-designed 3-HBA can not only suppress the deprotonation of organic cations and the following irreversible degradation route of amine-cation reaction but also inhibit the oxidation of I^-.

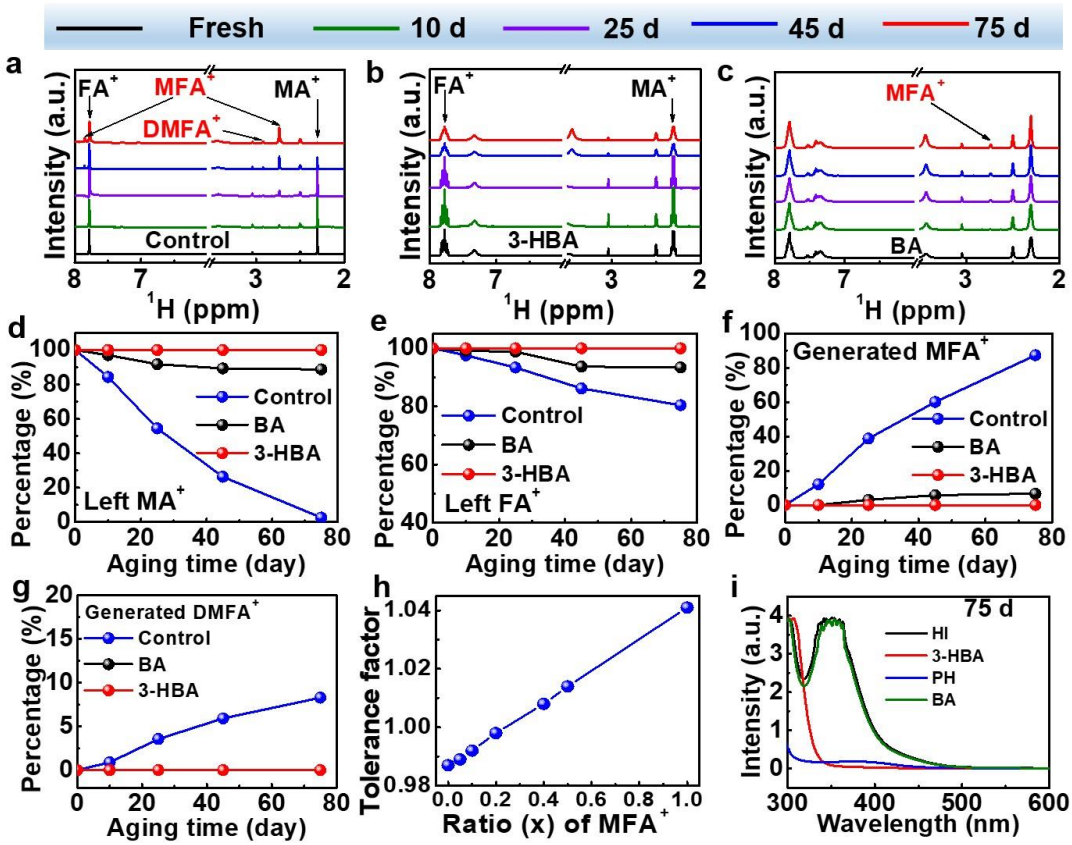

Figure 3. Degradation and stabilization mechanisms of the perovskite precursor solution. ^{1}H NMR spectra of the perovskite precursor solution of (a) control and modified perovskite precursor solutions with (b) 3-HBA, and (c) with BA aged for different times. Evolution of (d) left MA^{+}, (e) left FA^{+}, (f) generated MFA^{+}, and (g) $DMFA^{+}$ in the control perovskite precursor solution and modified perovskite precursor solutions with 3-HBA and BA aged for different times. (h) Tolerance factor of $FA_{1-x}(MFA)_xPbI_3$ perovskite. (i) UV-vis absorption spectra of the degraded commercial HI precursor solution without or with 3-HBA, PH, and BA as additives aged for 75 days.

The degradation of perovskite precursor solution is initially triggered by the deprotonation of organic cations, as discussed above and shown in reaction (i) in **Figure 4a**. Subsequently, the formed methylamine (MA) can nucleophilically attack the methine carbon of FA^{+} and then NH_3 is eliminated, which generates the MFAI product, as presented in reaction (ii).[11] Afterwards, the DMFAI will be produced by the further nucleophilic addition of methylamine to methine carbon of MFA^{+} and subsequent

elimination of NH_3, as illustrated in reaction (iii).[11] The reaction (iv) shows the deprotonation of FAI. The reactions (i)-(iv) are the main routes of chemical decomposition of mixed FA/MA-based perovskite precursor solution. The above decomposition reactions must be blocked for realizing long-term stable precursor solutions for the reproducible fabrication of efficient and stable PSCs. As displayed in reaction (v), the I^- ions in the solution are oxidized to I_2. It can be found from reaction (vi) that the 3-HBA can ionize to produce protons. In addition, 3-HBA can reduce the formed I_2 to I^- through reaction (v) during which H^+ is produced. The generated H^+ ions can inhibit the deprotonation of organic cations and thus the following irreversible amine-cation reaction is effectively suppressed. In brief, 3-HBA can stabilize the precursor solution by suppressing the deprotonation of organic cations and thus restraining irreversible amine-cation degradation reaction as well as inhibit the formation of I_2 via reducing I_2 back into I^-. **Figure 4b** schematically illustrates the effect of 3-HBA on the phase stability of perovskite films based on the solutions without and with 3-HBA. The α-$FAPbI_3$ film can be obtained based on the fresh precursor solution due to the presence of enough MA^+. After the precursor is aged, δ-$FAPbI_3$ is formed because of the consumption of small-size MA^+ and the generation of large-size organic cations (MFA^+ and $DMFA^+$). Upon the incorporation of 3-HBA in precursor, the α-$FAPbI_3$ film can still be obtained as the fresh control solution even if the solution is aged. It needs to be stressed that the -$NHNH_2$ can form hydrogen bond with halide ions and the -COOH can coordinate with undercoordinated Pb^{2+}, which results in effective passivation of the defects at GBs of perovskite films. The defect passivation effect will be discussed below.

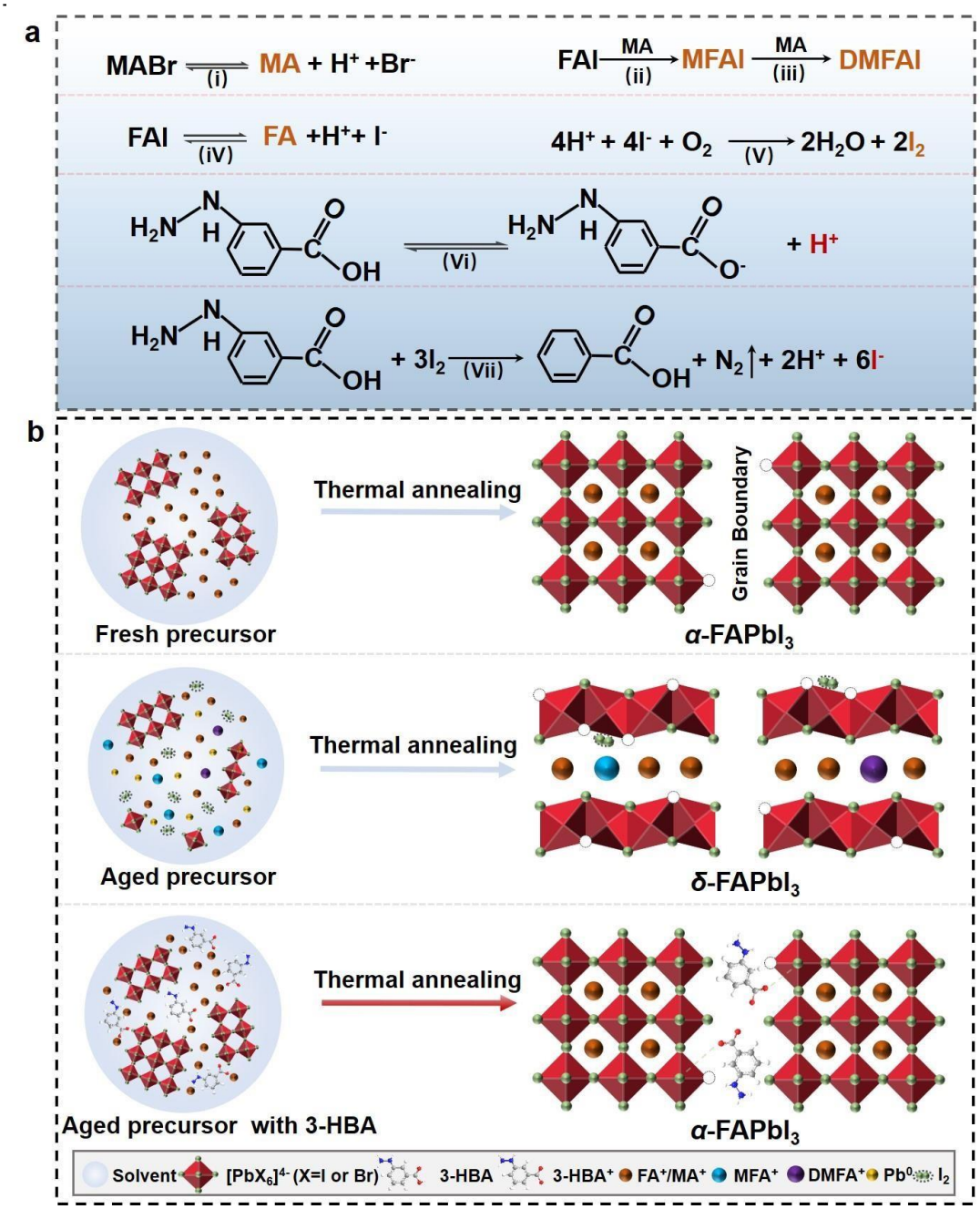

Figure 4. Chemical reactions involved in degradation and stabilization of perovskite precursor solution as well as a schematic illustration of phase stability improvement. (a) Degradation mechanism of mixed-organic-cation perovskite precursor solution and inhibition degradation mechanism by the synergistic effect of -COOH and -$NHNH_2$ in 3-HBA molecule. Reaction (i) is the deprotonation reaction of MABr. Reaction (ii) is the addition-elimination reaction between MA and FAI. Reaction (iii) is the addition-elimination reaction between MA and MFAI. Reaction (iv) is the deprotonation reaction of FAI. Reaction (v) is the oxidization of I^- by O_2.

Reaction (vi) is equilibrium proton ionization reaction of 3-HBA. Reaction (vii) is the reduction reaction between 3-HBA and I_2. (b) Schematic illustration of the suppression of the formation of yellow δ-$FAPbI_3$ with 3-HBA.

Chemical interaction and defect passivation

XPS spectrum shows the peaks of O=C-O and C-C from 3-HBA in the perovskite film using the fresh solution with 3-HBA (**Figure 5a**), which confirm the presence of 3-HBA in the final perovskite film. In **Figure 5b**, the binding energies of Pb $4f_{5/2}$ and Pb $4f_{7/2}$ are increased from 142.59 eV and 137.73 eV to 142.83 eV and 137.97 eV, respectively, after the addition of 3-HBA, which is coordination interaction between -COOH and undercoordinated Pb^{2+}.[36] From Fourier transform infrared (FTIR) spectra in **Figure 5c** and **Figure S21**, the stretching vibration peak (1770 cm^{-1}) of the carbonyl (C=O) in 3-HBA is shifted to a lower wavenumber (1714 cm^{-1}) upon interaction with PbI_2. This also shows the strong chemical interaction of 3-HBA with Pb^{2+}, which is in good accordance with the above XPS result. Subsequently, the interaction between 3-HBA with Pb^{2+} is further consolidated by the NMR spectra of 3-HBA and 3-HBA+PbI_2. As shown in **Figure 5d**, the ^1H NMR peak of -COOH in bare 3-HBA (10.23 ppm) is shifted to a lower chemical shift (9.91 ppm) in the 3-HBA+PbI_2 sample. At the same time, it is found that the ^{13}C NMR peak at 167.56 ppm of bare 3-HBA belonging to the carboxyl group, is shifted to 167.51 ppm after the introduction of PbI_2 (**Figure 5e**). The above XPS, FTIR, and NMR results together strongly demonstrate the strong chemical interaction between 3-HBA and Pb^{2+}. The high-resolution transmission electron microscope (HRTEM) measurement was performed to reveal the location and distribution of additive molecules in the final perovskite film. As shown in **Figure S22**, the amorphous component between perovskite grains should belong to 3-HBA, which is indicative of the presence of 3-HBA at GBs of perovskite films. It is inferred that 3-HBA can effectively passivate the undercoordinated Pb^{2+} defects at GBs, as proved in the following.

Space-charge-limited current (SCLC) measurement was carried out to explore the effect of 3-HBA modification on trap density and carrier recombination (**Figure 5f and S23**). The defect density is calculated as in our previous reports.[37] The electron trap state density in 3-HBA-modified perovskite film (2.0×10^{15} cm^{-3}) is lower than that in pristine film (6.6×10^{15} cm^{-3}). Meanwhile, the 3-HBA-modified perovskite film (2.6×10^{15} cm^{-3}) exhibits reduced hole trap state density as compared to the bare film (3.9×10^{15} cm^{-3}). It suggests that 3-HBA can effectively mitigate nonradiative recombination by passivating the defects at GBs and reducing trap state density. The effect of 3-HBA passivation on the carrier recombination of perovskite films based on fresh and aged precursor solutions was investigated through measuring the time-resolved photoluminescence (TRPL) spectra (**Figure 5g**). As presented in **Table S3**, the carrier lifetime of the perovskite film from the control solution aged for 75 days (51.77 ns) is reduced by 57% compared with that of the perovskite film fabricated from the fresh control solution (119.15 ns). However, the carrier lifetime is decreased from 809.97 ns of the perovskite film from the fresh target solution to 635.33 ns of the perovskite film from the aged target solution for 75 days, which corresponds to a reduction of 16%. On the one hand, for the fresh solution, the carrier lifetime is significantly increased from 119.15 ns to 608.64 ns after the incorporation of 3-HBA. This proves the effective passivation of 3-HBA for the defects at GBs, which is consistent with reduced defect density. On the other hand, the degradation rate of the control solution is much faster than that of the target solution because 3-HBA can not only suppress the oxidation of I^- but also can inhibit the deprotonation of organic cations and thus blocks the addition-elimination reaction between organic amine and organic cation.

We performed Kelvin probe force microscopy (KPFM) measurement to characterize the surface potential of the perovskite film without and with 3-HBA. The average local surface potentials are increased from -109.01 mV for the control film to +245.19 mV for the 3-HBA modified film (**Figure S24)**, indicating that the 3-HBA modification has a positive effect on the band edge of grain boundaries and can

promote carrier transport in perovskite film. Subsequently, we gained insights into the carrier recombination of NiO_x-based inverted PSCs without and with 3-HBA using triple cation perovskite as the absorber. As illustrated in **Figure S25**, introducing 3-HBA can effectively reduce the charge transfer and transfer resistance (R_{ct}) and increase the charge recombination resistance (R_{rec}), which is attributed to the improved carrier transport, reduced defect density, and increased carrier lifetime. The improved carrier transport and transfer are also demonstrated by the reduced carrier lifetime of the target device compared to the control device as shown in the transient photocurrent decay curve (**Figure S26)**. The increased carrier lifetime from 0.242 μs to 3.81 μs shows that the nonradiative recombination is significantly reduced due to reduced defect density and boosted carrier lifetime after the passivation by 3-HBA (**Figure 5h**). As revealed in the dark *J-V* curves in **Figure S27**, the smaller leakage current can be observed in the 3-HBA modified device in comparison with the control device, which further indicates that the charge transfer is improved and the charge recombination loss is reduced after the modification of 3-HBA. The V_{OC} is plotted as a function of light intensity for the control and target inverted devices based on triple cation perovskite (**Figure 5i**). The ideality factor *n* (1.15) of the 3-HBA modified device is closer to 1 than that of the control device (1.71), indicating that the carrier non-radiative recombination is greatly reduced upon the introduction of 3-HBA. In a word, stabilizing precursor solution by inhibiting the oxidization of iodide as well as the deprotonation of organic cations and suppressing nonradiative recombination by passivating the defects at GB are achieved simultaneously after the addition of 3-HBA.

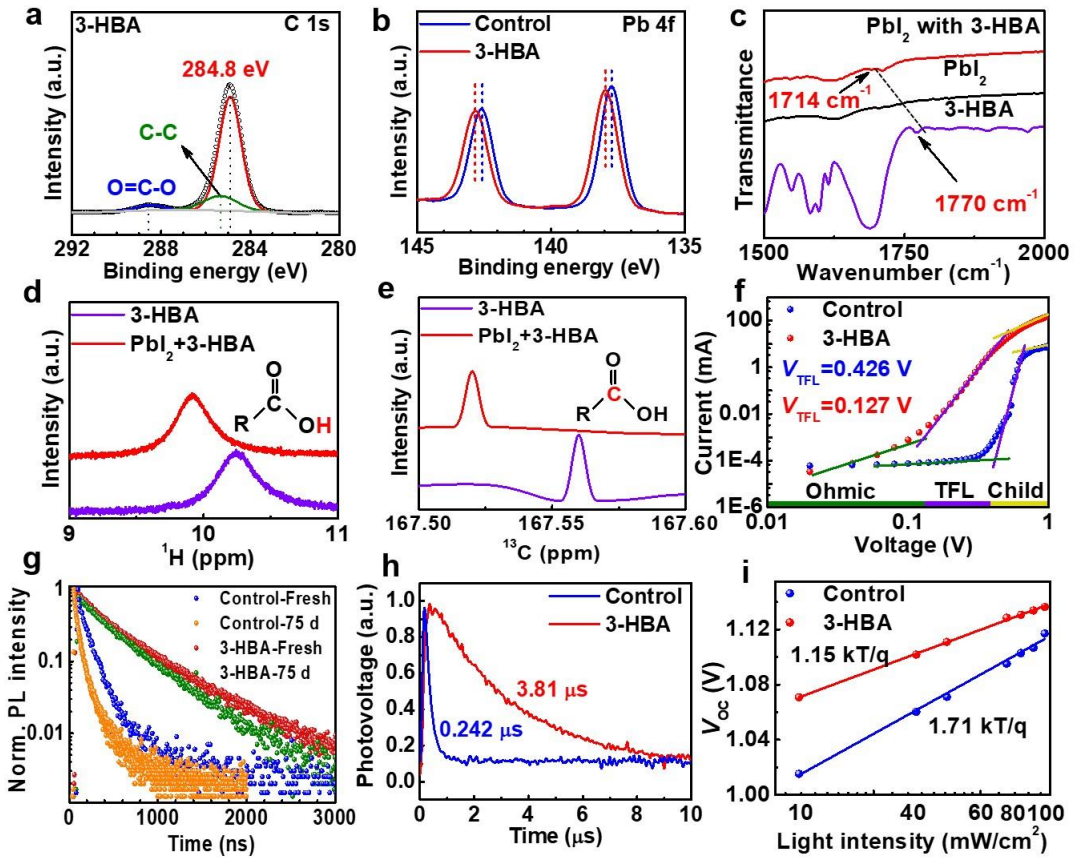

Figure 5. Characterizations of chemical interaction, trap state density, and carrier recombination. (a) C 1s and (b) Pb 4f XPS spectra of the perovskite films based on the fresh precursor solutions without and with 3-HBA. (c) FTIR spectra ranging from 1500 cm^{-1} to 2000 cm^{-1} of 3-HBA, PbI_2, and PbI_2+3-HBA. (d) ^{1}H NMR and (e) ^{13}C NMR spectra of 3-HBA and PbI_2+3-HBA solutions dissolved into DMSO-d6. (f) Dark *I-V* curves of the electron-only devices (ITO/SnO_2/Perovskite/PCBM/Ag). (g) TRPL spectra of the perovskite films based on the fresh and 75 days-aged precursor solutions without and with 3-HBA. (h) Transient photovoltage decay curves of the control and target inverted devices based on triple cation perovskite. (i) V_{OC} as a function of light intensity for the control and 3-HBA modified inverted devices based on triple cation perovskite.

Photovoltaic performance

Encouraged by these beneficial effects on the stabilizing of the precursor solution and the passivation of defects, we fabricated inverted

PSCs with the following structure : ITO/NiO_x/Al_2O_3/PTAA/PEAI/perovskite without or with 3-HBA/PCBM/BCP/Ag (where perovskite consists of $Cs_{0.05}(FA_{0.83}MA_{0.17})_{0.95}Pb(I_{0.83}Br_{0.17})_3$) to study the effect of 3-HBA on photovoltaic performance,. As shown in **Figure 6a**, Al_2O_3 was employed to block the electron back transfer from perovskite layer to hole transport layer. PTAA was used to modulate the interfacial energy band alignment between the NiO_x layer and the perovskite layer.[38] The concentration of 3-HBA was optimum for (0.16 mg/mL(**Figure S28**). As exhibited in **Figure 6b** and **Table S4**, the inverted target device with triple-cation perovskite gives a PCE of 21.75%, with a short-circuit current density (J_{SC}) of 23.20 mA/cm^2, an open-circuit voltage (V_{OC}) of 1.149 V, and a fill factor (FF) of 0.815. In contrast, the inverted control device with triple-cation perovskite produces a PCE of 20.49%, with a J_{SC} of 22.61 mA/cm^2, a V_{OC} of 1.129 V, and an FF of 0.807. The improved PCE is mainly the result of increased V_{OC} and FF, which should be put down to the effective passivation of 3-HBA for the defects at GBs as reflected by reduced defect density and increased carrier lifetime. To further increase J_{SC}, MA-free mixed cation perovskite $FA_{0.95}Cs_{0.05}PbI_3$ with a narrower bandgap was utilized to fabricate inverted devices and the effect of concentrations of 3-HBA on device performance is shown in **Figure S29**. As presented in **Figure 6c and Table S5**, the best-performing inverted target device with FACs-based perovskite delivers a PCE of 23.49% in reverse scan (J_{SC} of 25.38 mA/cm^2, a V_{OC} of 1.138 V, and an FF of 0.814) and a PCE of 23.25% in forward scan (J_{SC} of 25.38 mA/cm^2, a V_{OC} of 1.140 V, and an FF of 0.803). To the best of our knowledge, our achieved efficiency (23.49%) is the record value ever reported for NiO_x-based inverted PSCs (**Table S6**). However, the champion inverted control device with FACs-based perovskite exhibits a reverse-scanned PCE of 21.56% (J_{SC} of 24.87 mA/cm^2, a V_{OC} of 1.127 V, and an FF of 0.769) and a forward-scanned PCE of 20.87% (J_{SC} of 24.90 mA/cm^2, a V_{OC} of 1.116 V, and an FF of 0.751). The hysteresis is remarkably suppressed after the doping by 3-HBA. More importantly, the inverted target device achieves an attractive certified PCE of up to 21.52% (Certified chart in **Figure S30**) together with (J_{SC} of 25.47

mA/cm^2, a V_{OC} of 1.131 V, and an FF of 0.755). The integrated current density is well-consistent with the J_{SC} from *J-V* curve (**Figure S31**). To further demonstrate the universal defect passivation function of 3-HBA regardless of device architecture and perovskite composition, we also fabricated SnO_2-based regular PSCs using nominal $FA_{0.97}Cs_{0.03}PbI_3$ perovskite films prepared by sequential deposition. The PCE is improved from 21.94% for the control device to 23.48% for the target device (**Figure S32** and **Table S7**). The above results indicate that 3-HBA is an universal defect passivator which is independent of device structure and perovskite composition. Finally, it can be concluded that 3-HBA can not only stabilize precursor solution but also improve photovoltaic performance by passivating the defects at GBs.

The stability of the control and 3-HBA modified films and devices were tested. **Figure S33** pictures of the morphological change to reveal the effect of 3-HBA modification on the moisture stability of perovskite films. We can observe that the control film gradually turns yellow as the aging time increases while the 3-HBA-modified film remains black even if after 20 days. As can be seen from SEM images after aging for 20 days (**Figure S34**), the perovskite grains at some regions have decomposed completely and the ITO substrate is exposed whereas the target film still has a complete and flat morphology, which suggests that much more severe decomposition can be found in the control film than the target film. In addition, it can be found in **Figure S35** that just slightly reduced UV-vis absorption intensity is observed for the aged target film with respect to the fresh target film while the control film exhibits a marked decrease in UV-vis absorption intensity after being aged for 20 days. Furthermore, we also further confirmed the more rapid degradation of the control film than the modified film through measuring XRD patterns. As shown in **Figure S36**, the control film is almost fully converted into the yellow phase after 20 days of aging while only a tiny amount of yellow phase is produced and the peak intensity of PbI_2 slightly increases for the target film. In one word, the above results strongly demonstrate that the moisture stability of perovskite films is markedly improved after the incorporation of 3-HBA.

As for the stability of unencapsulated PSCs, the target device maintained 96% of its initial PCE after storing in the dark condition with a relative humidity of 10-20% for 2016 h while the control device retained only 57% after 1344 h of aging (**Figure 6d and Figure S37**). In addition, we also performed thermal stability measurements in the dark at 85 °C in a nitrogen-filled glove box (**Figure 6e** and **Figure S38**). The target device degraded by 28% after 672 h, while the control device degraded by 45% just after 240 h. We examined the long-term operational stability of the unsealed control and target devices by maximum power point tracking under continuous one sunlight illumination (**Figure 6f**). The PCE of the control device degraded to 65% of its original efficiency after 385 h whereas the PCE of the target device degrades to 94% of its initial efficiency after 601 h. The reduced trap-assisted nonradiative recombination due to effective defect passivation by 3-HBA should be mainly responsible for enhanced film and device stability.[14,27,36,39]

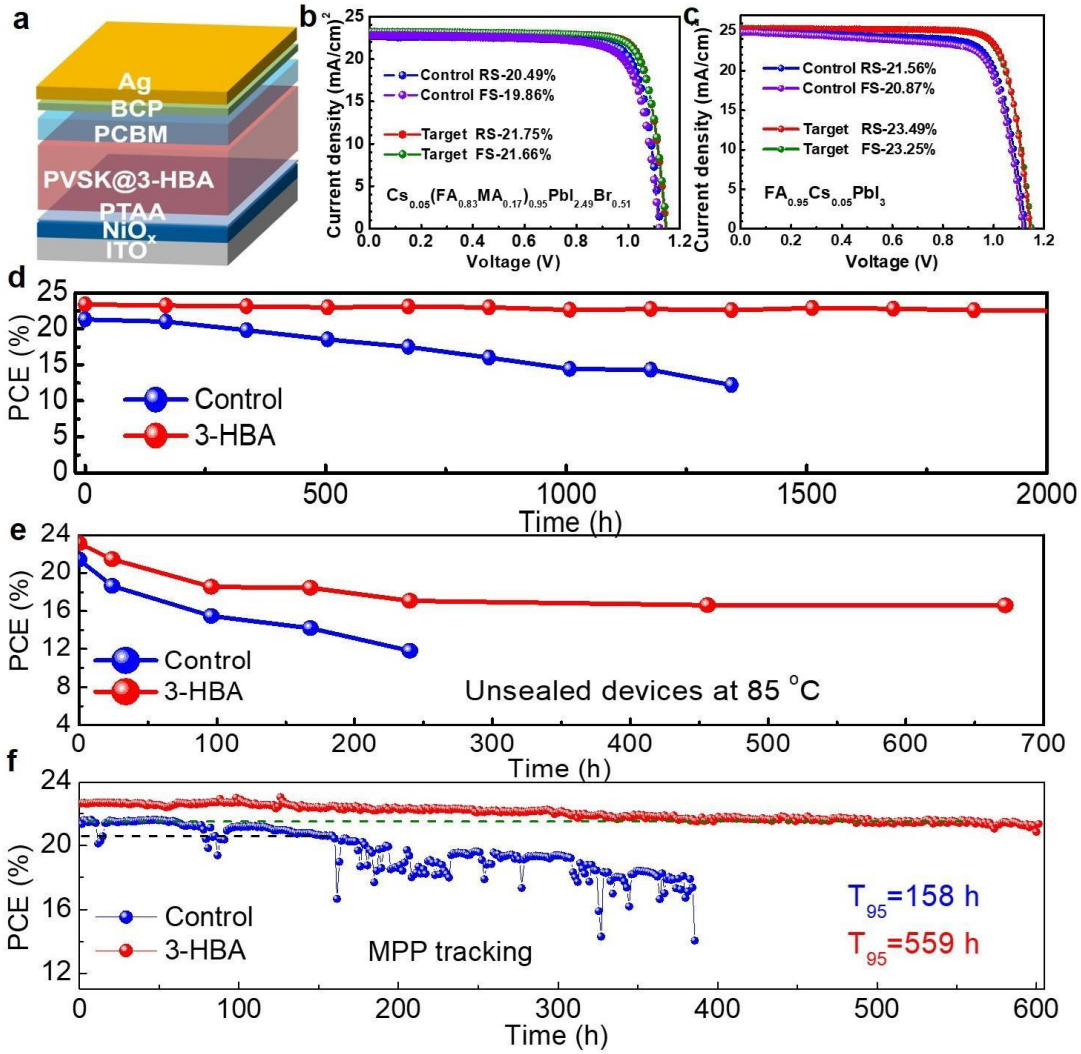

Figure 6. Device structure and performance of perovskite solar cells using 3-HBA. (a) The device structure of NiO_x-based inverted PSC in this work. (b) *J-V* curves of the champion inverted control and target devices based on triple-cation perovskite $Cs_{0.05}(FA_{0.83}MA_{0.17})_{0.95}Pb(I_{0.83}Br_{0.17})_3$ films. (c) *J-V* curves of the champion inverted control and target devices based on MA-free perovskite $FA_{0.95}Cs_{0.05}PbI_3$ films. (d) Moisture stability of the unsealed control and target devices aged under a relative humidity of 10%-20% in the dark. (e) Thermal stability in the nitrogen-filled glove box at 85°C of the unsealed control and target devices aged in the dark. (f) Maximum power point tracking for the control and target inverted devices based on double-cation perovskites under one sun illumination of 100 mW/cm^2 provided by white light LED.

Conclusions

In summary, we have demonstrated a simple and effective precursor stabilization and defect passivation strategy where multifunctional 3-HBA containing both -COOH and -$NHNH_2$ functional groups is incorporated into perovskite precursor solution. We have shown that the oxidation of I^-, the deprotonation of organic cations and the irreversible degradation route of amine-cation reaction are the main responsibles for the degradation of mixed-organic-cation metal halide perovskite precursor solution. It is demonstrated that the -$NHNH_2$ in 3-HBA can reduce I_2 defects back to I^- and thus suppress the oxidation of I^-. At the same time, it is uncovered that -COOH in 3-HBA as weak acid can produce hydrogen proton by reversible equilibrium ionization reaction, which can inhibit the deprotonation of organic cations and subsequent amine-cation reaction. The synergistic effect of -$NHNH_2$ and -COOH has been shown to enable simultaneous suppression of the above three degradation reactions. Moreover, the 3-HBA is certified to be one universal defect passivator regardless of perovskite composition and device configuration. As a result, the resulting NiO_x-based inverted solar cell produced an attractive efficiency of 23.5%, which is the highest value ever reported for an NiO_x-based inverted PSC. The modified device with 3-HBA maintained 72% of the initial efficiency after aging at 85 ℃ for 672 h and 94% of the initial efficiency after maximum power point tracking under continuous illumination for 601 h. The precursor solution stabilization and defect passivation strategy developed in this work will contribute to accelerate the industrialization of perovskite optoelectronic devices.

Methods

Materials. All chemicals and solvents were used as received without further purification. SnO_2 colloidal solution (tin (IV) oxide, 15% in H_2O colloidal dispersion) was purchased from Alfa Aesar. Bis(trifluoromethane) sulfonimide lithium salt

(Li-TFSI, 99%), and poly(triaryl amine) (PTAA, molecular weight distribution：6000-15000) were purchased from Xi'an Polymer Light Technology Corp. Methylammonium bromide (MABr, 99.9%), methylammonium iodide (MAI, 99.9%), methylamine hydrochloride (MACl, 99.9%), formamidine hydroiodide (FAI, 99.9%), cesium iodide (CsI, 99.999%), lead (II) iodide (PbI_2, 99.99%), lead (II) bromide ($PbBr_2$, 99.99%), Spiro-OMeTAD (99.86%), phenethylammonium iodide (PEAI, 99.9%) and bathocuproine (BCP) were bought from Advanced Election Technology Co. Ltd. 4-Tert-butylpyridine (*t*-BP, 99%), chlorobenzene (CB, >99.9%), N, N-dimethylformamide (DMF, 99.8%), isopropanol (IPA, 99.5%), dimethyl sulfoxide (DMSO, 99.8%), acetonitrile (ACN, 99.8%) and aluminum oxide nanoparticle dispersion (Al_2O_3, 20 wt.% in isopropanol) were purchased from Sigma-Aldrich. Dimethyl sulfoxide-d6 (DMSO-d6, 99.9%), 3-hydrazinobenzoic acid (3-HBA, 98%), phenylhydrazine (PH, 98.0%), benzoic acid (BA, 99.9%), benzene (99.5%), formic acid (HCOOH, ≥99%), 3-methylbenzoic acid (3-MBA, 99.0%) and 3-aminobenzoic acid (3-ABA, 98%) were purchased from Macklin. [6,6]-phenyl C_{61} butyric acid methyl ester ($PC_{61}BM$) was obtained from Nano-C. Nickel(II) nitrate hexahydrate ($Ni(NO_3)_2 \cdot 6H_2O$, 98%) was bought from Aladdin. NiO_x nanoparticles (NPs) were synthesized according to the previous work.[40]

Fabrication of NiO_x-based inverted perovskite solar cells. ITO-coated glass substrates were etched by laser. The etched ITO glass was ultrasonically cleaned for 15 min using detergent, deionized water (twice), and ethanol (twice), sequentially. ITO-coated glass substrates were treated by ultraviolet–ozone (UVO) for 30 min. Then, the 30 mg/mL NiO_x NPs aqueous ink was prepared by dispersing as-prepared NiO_x NPs into deionized water and then spin-coated on ITO glass at 4000 rpm for 30 s. The NiO_x films were annealed at 150 °C for 10 min under ambient conditions. And then, obtained NiO_x films were immediately transferred into the glove box filled with nitrogen. 1 mg/mL PTAA solution in CB was spin-coated onto NiO_x films at 6000 rpm for 30 s. Al_2O_3 dispersion solution was prepared by diluting 20 μL 20 wt.% stock solution in isopropanol with 1 mL IPA and then was spin-coated on PTAA films at

5000 rpm for 30 s. 1 mg/mL PEAI solution in IPA was spin-coated on ITO/NiO_x/PTAA/Al_2O_3 films at 5000 rpm for 30 s. For triple-cation perovskite films, 1.4 M perovskite precursor solution was prepared through dissolving 189.8 mg FAI, 18.2 mg CsI, 25.3 mg MABr, 568.0 mg PbI_2, 87.4 mg $PbBr_2$, and 3-HBA (0, 0.04, 0.08, 0.16 and 0.32 mg/mL) in mixed solvents of DMF and DMSO (v/v: 4:1). The perovskite precursor solution was spin-coated at 2000 rpm for 10 s and then at 4000 rpm for 30 s. During the second spinning routine step, 120 μL CB was dropped onto the spinning substrates at 5 s before ending the program. The perovskite films were annealed at 110 °C for 60 min. For $FA_{0.95}Cs_{0.05}PbI_3$ perovskite films, 1.4 M perovskite precursor solution was prepared through dissolving 228.4 mg FAI, 18.2 mg CsI, and 645.4 mg PbI_2, and 3-HBA (0, 0.04, 0.08, 0.16 and 0.32 mg/mL) in mixed solvents of DMF and DMSO (v/v: 4:1). The perovskite precursor solution was spin-coated at 2000 rpm for 10 s and then at 4000 rpm for 40 s. During the second spinning routine step, 150 μL CB was dropped onto the perovskite film at 5 s before ending the program. The resultant wet perovskite films were annealed at 100 °C for 30 min. Subsequently, a $PC_{61}BM$ solution in CB (23 mg/mL) was spin-coated on the perovskite films at 2500 rpm for 40 s. Thenafter, the BCP solution in IPA (5 mg/mL) was spin-coated on $PC_{61}BM$ film at 5000 rpm for 30 s. Finally, a 100 nm Ag electrode was thermally evaporated on the BCP film under a vacuum of 7.5×10^{-5} Pa through a shadow mask.

Fabrication of SnO_2-based regular perovskite solar cells. The ITO glass was cleaned as described above. The ITO substrates were exposed to UVO for 30 min. The 3 wt% SnO_2 aqueous colloidal solution, prepared by diluting 15 wt% SnO_2 aqueous colloidal dispersion with deionized water, was spin-coated on the ITO-coated glass substrates at 4000 rpm for 30 s and then SnO_2 film was annealed on a hot plate in ambient air at 150 °C for 30 min. After the film cooled down to room temperature, the resultant SnO_2 film was treated by UVO for 10 min, and then transferred to a nitrogen-filled glove box. After that, a solution of PbI_2 (670.75 mg), CsI (11.69 mg), and 3-HBA (0, 0.05, 0.075 and 0.1 mg/mL) in a mixed solvent of DMF/DMSO (9:1,

volume ratio) was spin-coated onto SnO_2 film at 1500 rpm for 30 s.

The resulting SnO_2 film was annealed at 70 °C for 1 min. After PbI_2 cooled down to room temperature, the solution of FAI (90 mg) and MACl (16 mg) in 1 mL IPA was spin-coated onto the PbI_2 film at 2300 rpm for 30 s. The obtained perovskite film was annealed at 150 °C for 15 min in ambient conditions (30–40% humidity). The hole transporting layer was deposited on top of the perovskite layer at 4000 rpm for 30 s by spin-coating a Spiro-OMeTAD solution, which consisted of 72.3 mg Spiro-OMeTAD, 35 µL bis(trifluoromethane) sulfonimide lithium salt (Li-TFSI) stock solution (260 mg Li-TFSI in 1 mL acetonitrile), 30 µL *t*-BP, and 1 mL CB. Finally, a 100-nm-thick Ag electrode was thermally evaporated on the BCP film under a vacuum of 7.5×10^{-5} Pa by using a shadow mask.

Characterizations. UV-visible absorption spectra were measured on a Shimadzu UV-1900 spectrophotometer. Fourier transform infrared spectroscopy (FTIR) spectra were recorded on a Thermo-Fisher Nicolet iS50 Infrared Fourier transform microscope. X-ray diffraction (XRD) patterns were measured on a Rigaku SmartLab (9KW) X-ray diffractometer with Cu Kα radiation (0.154 nm). NMR spectra were measured with a Bruker AVANCE 400 instrument operating at 400 MHz at 298 K. X-ray photoelectron spectra (XPS) and Ultraviolet photoelectron spectroscopy (UPS) measurements were carried out on ESCALAB 250Xi. Time-resolved photoluminescence (TRPL) and steady-state photoluminescence (SSPL) spectra were acquired by employing the FLS980 Series of Fluorescence Spectrometers with an excitation wavelength of 480 nm. The SEM images were obtained via the field-emission scanning electron microscope (JEOL 7610F) using secondary electrons. The scanning voltage is 5.5 kV. Agilent 5500 scanning probe microscopy was utilized for AFM topography and KPFM in tapping mode, whereas CS-AFM in contact mode with 1 V applied bias. The HR-TEM images were obtained using a high-resolution transmission electron microscope (JEM-2100F, Japan) in high-resolution mode. Electrochemical impedance spectroscopy (EIS) was measured on an Electrochemical Workstation (China) and the data were processed using Z-View program. TPV and TPC measurements were performed as follows: the devices were illuminated with

laser pulses (532 nm, 100 mJ, 6 ns width from an Nd: YAG laser), and then the decay of signals was collected through a 1 GHz Agilent digital oscilloscope (DSO-X3102A) with the input impedance of 1 MΩ/50 Ω. *J–V* curves in forward scan (from -0.1 to 1.2 V) and reverse scan (from 1.2 to -0.1 V) were obtained using a solar simulator equipped (150W, SolarIV-150A) with a Keithley 2400 source meter. Light intensity was calibrated to AM 1.5G one sun (100 mW/cm^2) using a NIM calibrated standard Si solar cell (QE-B1). The black metal mask was used to define the effective active area of devices (0.08 cm^2). Incident photon-to-current efficiency (IPCE) measurement was performed through a Newport Instruments system (Newport-74125) coupled with a lock-in amplifier and a 300 W Xenon lamp. For the continuous illumination MPP tracking stability test of the device, a customized stability test system including aLED light source (Meitong, Tianjin) and a continuous test program for the aging test was adopted. The light intensity of the LED light source was calibrated by the steady-state current of PSCs under the solar simulator.

Acknowledgments

This work was supported by the National Natural Science Foundation of China (Grant Nos. 62004058, U21A2076, 21701041, 52071048), Nature Science Foundation of Hebei Province (F2020202022), the Open Fund of the State Key Laboratory of Integrated Optoelectronics (IOSKL2020KF09), State Key Laboratory of Reliability and Intelligence of Electrical Equipment (No. EERI_PI20200005). This work was also supported by Support plan for Overseas Students to Return to China for Entrepreneurship and Innovation (Grant No. cx2020003), the Fundamental Research Funds for the Central Universities (Grant No. 2020CDJ-LHZZ-074), and Natural Science Foundation of Chongqing (Grant No. cstc2020jcyj-msxmX0629).

Conflict of Interest

The authors declare no conflict of interest.

References

1 https://www.nrel.gov/pv/assets/pdfs/best-research-cell-efficiencies-rev211214.pdf.

2 Chen, S., Xiao, X., Gu, H. & Huang, J. Iodine reduction for reproducible and high-performance perovskite solar cells and modules. *Science Advances* **7**, eabe8130 (2021).

3 Wang, X. *et al.* Perovskite Solution Aging: What Happened and How to Inhibit? *Chem* **6**, 1369-1378, doi:https://doi.org/10.1016/j.chempr.2020.02.016 (2020).

4 Kim, J. *et al.* Unveiling the Relationship between the Perovskite Precursor Solution and the Resulting Device Performance. *Journal of the American Chemical Society* **142**, 6251-6260, doi:10.1021/jacs.0c00411 (2020).

5 Ozaki, M. *et al.* A Purified, Solvent-Intercalated Precursor Complex for Wide-Process - Window Fabrication of Efficient Perovskite Solar Cells and Modules. *Angewandte Chemie International Edition* **58**, 9389-9393 (2019).

6 Shin, G. S., Kim, S. G., Zhang, Y. & Park, N. G. A correlation between iodoplumbate and photovoltaic performance of perovskite solar cells observed by precursor solution aging. *Small Methods* **4**, 1900398 (2020).

7 McMeekin, D. P. *et al.* Crystallization Kinetics and Morphology Control of Formamidinium–Cesium Mixed-Cation Lead Mixed-Halide Perovskite via Tunability of the Colloidal Precursor Solution. *Advanced Materials* **29**, 1607039 (2017).

8 Dong, Q. *et al.* Critical Role of Organoamines in the Irreversible Degradation of a Metal Halide Perovskite Precursor Colloid: Mechanism and Inhibiting Strategy. *ACS Energy Letters* **7**, 481-489, doi:10.1021/acsenergylett.1c02449 (2022).

9 Noel, N. K. *et al.* Unveiling the Influence of pH on the Crystallization of Hybrid Perovskites, Delivering Low Voltage Loss Photovoltaics. *Joule* **1**, 328-343, doi:https://doi.org/10.1016/j.joule.2017.09.009 (2017).

10 Dou, B. *et al.* Degradation of Highly Alloyed Metal Halide Perovskite Precursor Inks: Mechanism and Storage Solutions. *ACS Energy Letters* **3**, 979-985, doi:10.1021/acsenergylett.8b00305 (2018).

11 Valenzano, V. *et al.* Methylammonium-formamidinium reactivity in aged organometal halide perovskite inks. *Cell Reports Physical Science* **2**, 100432, doi:https://doi.org/10.1016/j.xcrp.2021.100432 (2021).

12 Tsai, H. *et al.* Effect of precursor solution aging on the crystallinity and photovoltaic performance of perovskite solar cells. *Advanced Energy Materials* **7**, 1602159 (2017).

13 Wang, L. *et al.* A Eu³⁺-Eu²⁺ ion redox shuttle imparts operational durability to Pb-I perovskite solar cells. *Science* **363**, 265-270, doi:10.1126/science.aau5701 (2019).

14 Zhu, L. *et al.* Trap State Passivation by Rational Ligand Molecule Engineering toward Efficient and Stable Perovskite Solar Cells Exceeding 23% Efficiency. *Advanced Energy Materials* **11**, 2100529, doi:https://doi.org/10.1002/aenm.202100529 (2021).

15 Li, M. *et al.* Multifunctional Reductive Molecular Modulator toward Efficient and Stable Perovskite Solar Cells. *Solar RRL* **5**, 2100320, doi:https://doi.org/10.1002/solr.202100320 (2021).

16 Chen, J., He, D. & Park, N.-G. Methodologies for >30% Efficient Perovskite Solar Cells via Enhancement of Voltage and Fill Factor. *Solar RRL* **6**, 2100767, doi:https://doi.org/10.1002/solr.202100767 (2022).

17 Chen, J., He, D. & Park, N.-G. Methodologies for> 30% Efficient Perovskite Solar Cells via Enhancement of Voltage and Fill Factor. *Solar RRL* **6**, 2100767 (2022).

18 Hui, W. *et al.* Stabilizing black-phase formamidinium perovskite formation at room temperature and high humidity. *Science* **371**, 1359-1364 (2021).

19 Lu, H. *et al.* Vapor-assisted deposition of highly efficient, stable black-phase FAPbI3 perovskite solar cells. *Science* **370**, eabb8985 (2020).

20 Qin, M. *et al.* Fused-Ring Electron Acceptor ITIC-Th: A Novel Stabilizer for Halide Perovskite Precursor Solution. *Advanced Energy Materials* **8**, 1703399 (2018).

21 Min, H. *et al.* Stabilization of Precursor Solution and Perovskite Layer by Addition of Sulfur. *Advanced Energy Materials* **9**, 1803476, doi:https://doi.org/10.1002/aenm.201803476 (2019).

22 Chen, C. *et al.* Stabilizing Formamidinium Lead Iodide Perovskite Precursor Solution with Phenylboric Acid. *Solar RRL* **5**, 2000715, doi:10.1002/solr.202000715 (2021).

23 Dong, Q. *et al.* Critical Role of Organoamines in the Irreversible Degradation of a Metal Halide Perovskite Precursor Colloid: Mechanism and Inhibiting Strategy. *ACS Energy Letters*, 481-489, doi:10.1021/acsenergylett.1c02449 (2021).

24 Azmi, R. *et al.* Damp heat–stable perovskite solar cells with tailored-dimensionality 2D/3D heterojunctions. *Science* **0**, eabm5784, doi:doi:10.1126/science.abm5784.

25 Li, X. *et al.* Constructing heterojunctions by surface sulfidation for efficient inverted perovskite solar cells. *Science* **375**, 434-437, doi:doi:10.1126/science.abl5676 (2022).

26 Wang, K. *et al.* Isothermally crystallized perovskites at room-temperature. *Energy & Environmental Science* **13**, 3412-3422, doi:10.1039/D0EE01967D (2020).

27 Chen, J. & Park, N.-G. Causes and Solutions of Recombination in Perovskite Solar Cells. *Advanced Materials* **31**, 1803019, doi:https://doi.org/10.1002/adma.201803019 (2019).

28 Chen, J. & Park, N.-G. Materials and Methods for Interface Engineering toward Stable and Efficient Perovskite Solar Cells. *ACS Energy Letters* **5**, 2742-2786, doi:10.1021/acsenergylett.0c01240 (2020).

29 Zhang, W. *et al.* Enhanced optoelectronic quality of perovskite thin films with hypophosphorous acid for planar heterojunction solar cells. *Nature Communications* **6**, 10030, doi:10.1038/ncomms10030 (2015).

30 (!!! INVALID CITATION !!! 3, 16).

31 (!!! INVALID CITATION !!! 3, 15).

32 (!!! INVALID CITATION !!! 3, 15, 16).

33 (!!! INVALID CITATION !!! 32, 33).

34 (!!! INVALID CITATION !!! 2).

35 (!!! INVALID CITATION !!! 2, 34, 35).

36 Liu, B. *et al.* Interfacial Defect Passivation and Stress Release via Multi-Active-Site Ligand Anchoring Enables Efficient and Stable Methylammonium-Free Perovskite Solar Cells. *ACS Energy Letters* **6**, 2526-2538, doi:10.1021/acsenergylett.1c00794 (2021).

37 (!!! INVALID CITATION !!! 36, 37).

38 Wang, Y. *et al.* Cation-size mismatch and interface stabilization for efficient NiOx-based inverted perovskite solar cells with 21.9% efficiency. *Nano Energy* **88**, 106285, doi:https://doi.org/10.1016/j.nanoen.2021.106285 (2021).

39 Ono, L. K., Liu, S. & Qi, Y. Reducing Detrimental Defects for High-Performance Metal Halide Perovskite Solar Cells. *Angewandte Chemie International Edition* **59**, 6676-6698, doi:https://doi.org/10.1002/anie.201905521 (2020).

40 Zhang, H. *et al.* Toward All Room-Temperature, Solution-Processed, High-Performance Planar Perovskite Solar Cells: A New Scheme of Pyridine-Promoted Perovskite Formation. *Advanced Materials* **29**, 1604695, doi:https://doi.org/10.1002/adma.201604695 (2017).